ELSEVIER

Journal of Biomechanics 40 (2007) 2457–2466

JOURNAL OF BIOMECHANICS

www.elsevier.com/locate/jbiomech
www.JBiomech.com

Direct measurement of intervertebral disc maximum shear strain in six degrees of freedom: Motions that place disc tissue at risk of injury

J.J. Costi[a,*], I.A. Stokes[a], M. Gardner-Morse[a], J.P. Laible[b], H.M. Scoffone[c], J.C. Iatridis[d]

[a]Department of Orthopaedics & Rehabilitation, University of Vermont, Stafford Hall, Burlington, VT 05405-0084, USA
[b]Department of Civil & Environmental Engineering, University of Vermont, Burlington, VT, USA
[c]Department of Biomedical Engineering, Rensselaer Polytechnic Institute, Troy, NY, USA
[d]Department of Mechanical Engineering, University of Vermont, Burlington, VT, USA

Accepted 11 November 2006

Abstract

Human intervertebral disc specimens were tested to determine the regions of largest maximum shear strain (MSS) experienced by disc tissues in each of three principal displacements and three rotations, and to identify the physiological rotations and displacements that may place the disc at greatest risk for large tissue strains and injury. Tearing of disc annulus may be initiated by large interlamellar shear strains. Nine human lumbar discs were tagged with radiographic markers on the endplates, disc periphery and with a grid of wires in the mid-transverse plane and subjected to each of the six principal displacements and rotations. Stereo-radiographs were taken in each position and digitized for reconstruction of the three-dimensional position of each marker. Maximum tissue shear strains were calculated from relative marker displacements and normalized by the input displacement or rotation. Lateral shear, compression, and lateral bending were the motions that produced the mean (95% confidence interval) largest mean MSS of 9.6 (0.7)%/mm, 9.0 (0.5)%/mm, and 5.8 (1.6)%/°, respectively, and which occurred in the posterior, posterolateral and lateral peripheral regions of the disc. After taking into account the reported maximum physiological range of motion for each degree of freedom, motions producing the highest physiological MSS were lateral bending (57.8 (16.2)%) and flexion (38.3 (3.3)%), followed by lateral shear (14.4 (1.1)%) and compression (12.6 (0.7)%).

Keywords: Intervertebral disc; Shear strain; Six degree of freedom; Injury mechanism; Three-dimensional

1. Introduction

The intervertebral disc serves as a strong, flexible interface between adjacent vertebral bodies, and is responsible for transmitting loads in multiple directions while permitting movements of the spinal column. During certain motions, the disc is at risk of injury, of which posterolateral herniation, endplate failures and interlaminar tearing are probably the most clinically significant.

Epidemiological and in vitro studies have demonstrated that axial compression coupled with various combinations of flexion, and lateral bending can lead to disc injury (Adams et al., 1994, 2000; Adams and Hutton, 1982, 1985; Callaghan and Mcgill, 2001; Gordon et al., 1991; Kelsey et al., 1984; Marras et al., 1993; Miller et al., 1986). Usually, these injuries are caused by excessive motion of the lumbar segment, although similar injuries have also been caused by repetitive loading at lesser, more physiological amounts of motion (Adams and Hutton, 1983; Gordon et al., 1991; Shirazi-Adl, 1989; Steffen et al., 1998). While the posterolateral region seems to be most at risk for injury, other annular tears (circumferential and radial tears) are present by early adulthood, and these tears are associated with long-term development of disc degeneration and herniation (Vernon-Roberts et al., 1997; Vernon-Roberts and Pirie, 1977). It is believed that these tears may originate in response to variations in regional intra-discal shear strains (Goel et al., 1995), although the magnitude of these strains within the physiological range of motion is unknown.

*Corresponding author. Tel.: +61 8 8275 1751; fax: +61 8 8374 1998.
E-mail address: john.costi@rgh.sa.gov.au (J.J. Costi).

0021-9290/$ - see front matter © 2006 Elsevier Ltd. All rights reserved.
doi:10.1016/j.jbiomech.2006.11.006

Disc tissue internal deformation and strain have been estimated from displacements of markers in the mid-sagittal plane (Krag et al., 1987; Seroussi et al., 1989), and in the mid-transverse plane (Tsantrizos et al., 2005) during compression and bending loading. These studies were limited to two dimensions and while they provided useful insights into the internal behavior of the disc in compression and bending motions, axial rotation (Shirazi-Adl, 1989; Steffen et al., 1998) and shear loading (Marras et al., 2001; Mcgill et al., 2000; Norman et al., 1998) have been linked to increased back injury rates and these motions warrant investigation.

The primary objectives of this study were to determine the regions of largest shear strain experienced by disc tissues in each of three principal displacements and three rotations, and to identify the physiological rotations and displacements that may place the disc at greatest risk for large tissue strains and injury. Three-dimensional (3-D) principal strains were measured, from which the maximum shear strains were calculated, since these were considered to be the most likely to cause tissue failure.

2. Methods

The disc and the two adjoining hemi-vertebrae of nine lumbar human disc segments from three male spines (ages 29, 32 and 54 years, mean (SD) height 172.7 (2.5) cm and weight 79.5 (8.2) kg), levels T12/L1 × 2, L1/2 × 1, L2/3 × 3, L3/4 × 2, L4/5 × 1 were used in this study. According to Thompson's criteria (Thompson et al., 1990) for disc grade, seven discs were grade 1 (excellent), and two were between grades 2 and 3 (only the nucleus showed early signs of degeneration). Disc specimens were stored at −80 °C until they were prepared for testing by careful dissection of all soft tissue surrounding the motion segment and removal of the posterior elements.

Each disc and lower endplate was tagged with radiographic markers (Fig. 1). The lower endplate was marked by five 1.5 mm lead beads. One was placed at the endplate center at the end of a 2 mm diameter tunnel created by hand-drilling into the vertebral bodies until an increase in resistance was felt, indicating the endplate was reached. Four peripheral beads (anterior, posterior, left, right) were affixed to the margins of the endplate, as visualized during dissection, and all beads were fixed into position using cyanoacrylate. A local axis system was defined with its origin at the center marker of the lower endplate and axes defined by the four peripheral endplate markers. The positive axes directions were $+x$ = anterior, $+y$ = left lateral and $+z$ = superior (Fig. 1). The disc periphery was marked by stretching an elastic band around it, and gluing the ends together under tension, after fifteen to twenty 5 mm length tantalum wire segments had been inserted into the band at approximately equal intervals (Fig. 1a). Since the tension in the elastic band prevented it contacting the concave posterior region of the disc, markers within ±20° of the posterior point on the disc midline were excluded from subsequent analysis. The mid-transverse plane of the disc was marked by inserting two perpendicular rows of 0.25 mm diameter tantalum wires with 5 mm spacing between wires, to create a grid aligned at ±45° to the sagittal plane (Fig. 1b). Wires were inserted through each disc by threading it with a 18 G needle and needle-guide from one side to the other. Alignment of each wire was achieved with a translation and rotation stage (Tsantrizos et al., 2005).

Prior to insertion of the wires the hemi-vertebrae were embedded in radiolucent cups with polymethylmethacrylate cement. An alignment device ensured that the superior and inferior surfaces of each cup were parallel to each other and parallel to the mid-transverse plane of the disc. Axial and lateral radiographs were taken of each embedded specimen to identify the approximate location of the geometric center of the disc relative to the cups. This position was used as the center of rotation for the rotational tests described below.

For testing, each specimen was attached to the platens of a custom-made six degree of freedom (6 DOF) hexapod robot (Stokes et al., 2002). Radiolucent acrylic spacers above and below the specimen ensured an unobstructed view during stereo-radiography. The specimen was surrounded by a tank containing a 0.15 M phosphate buffered saline bath at 4 °C for the testing duration. The tank also served as a calibration object for stereo-radiography, having twelve 2 mm diameter lead beads mounted on it in known positions (Fig. 1).

Prior to testing, each specimen was equilibrated in the bath with a 100 N compressive preload for 3 h. After equilibration, stereo-radiographs of the specimen were taken and this position was considered as the initial datum position.

A sequence of 10 min ramp loadings consisting of five displacements (mean axial compression of 1.1 mm, mean left/right lateral shear of ±0.7 mm, and mean anterior/posterior shear of ±0.9 mm) and six rotations (mean flexion/extension of ±5.3°, mean left/right axial rotation of ±2.5°, and mean left/right lateral bending of ±4.8°) was applied to each specimen, with a 5-min dwell period at the datum position before stereo-radiographs were taken between each test. Finally, the specimen was returned to its datum position, and stereo-radiographed again. Axial compression was always the first displacement in the series, followed by axial rotation, anteroposterior shear, flexion/extension, lateral shear and lateral bending. The stereo-radiographs (Fig. 2) in each displaced position were made by use of a pair of X-ray tubes, each positioned at 60° to the mid-sagittal plane of the disc, and the tubes were raised and angled downwards at an angle of 45° (Fig. 1). Film cassettes were mounted behind the specimen such that they were perpendicular to the corresponding central X-ray beam.

The stereo-pairs of radiographs were scanned using a flatbed scanner at 600 dpi resolution (0.042 mm/pixel). The mean and 95% confidence interval (95% CI) precision RMS digitizing error was 0.045 mm (0.016 mm), which was similar to that reported by Tsantrizos et al. (2005) (0.042 mm). Landmarks were identified in each film and manually digitized using software written in Matlab (The Mathworks Inc., Natick, MA, USA). The Direct Linear Transformation (DLT) method as implemented in the Matlab routines dltfu.m and reconfu.m (Reinschmidt and van den Bogert, 1997) was used for the stereo-reconstruction of the 3-D coordinates of each landmark. Matching endplate beads were identified by the Hungarian method (Matlab functions hungarian.m and condass.m kindly provided by N. Börlin), and matching disc peripheral markers (tantalum wires in the elastic band) from each film were determined by the use of heuristic matching algorithms. The digitized positions of nine approximately equally spaced points defined the midline of each wire. The midlines of the wires were reconstructed by identifying matching points on the wires by interpolating along the corresponding images to find minimal DLT errors (Dansereau and Stokes, 1988). Subsequently, the closest approaches ('intersections') of wires were calculated to define points for tracking tissue displacements.

Displacements measured at the arbitrary positions (the tagged points in each disc) were first used to interpolate values at standardized grid positions (Fig. 3) so that they could be averaged between specimens. The regular, symmetrical, two dimensional (2-D) planar grid comprised of 148 four-noded quadrilateral elements with a total of 173 nodes. The periphery was defined by a 12th order polynomial fitted through averaged coordinates of the peripheral (elastic band) markers in un-displaced (datum) positions. Relative 3-D displacements of all coordinates (wires, endplate beads and circumferential markers) between displaced positions of the specimens were calculated and normalized by the respective input displacement (mm/mm) or rotation (mm/°).

For motions that were considered to be symmetrical about the mid-sagittal plane (axial rotation, lateral bending and lateral shear) the displacement data for the two complementary motions were pooled, after accounting for differences in sign, and the results are presented as if they were all for positive displacements (left axial rotation ($+Rz$), right lateral bending ($+Rx$), and left lateral shear ($+Ty$)).

The x and y planar and xy shear strains were calculated at each node of the planar grid from the relative nodal displacements, using linear shape (basis) functions and averaging neighboring elements. Strain in the

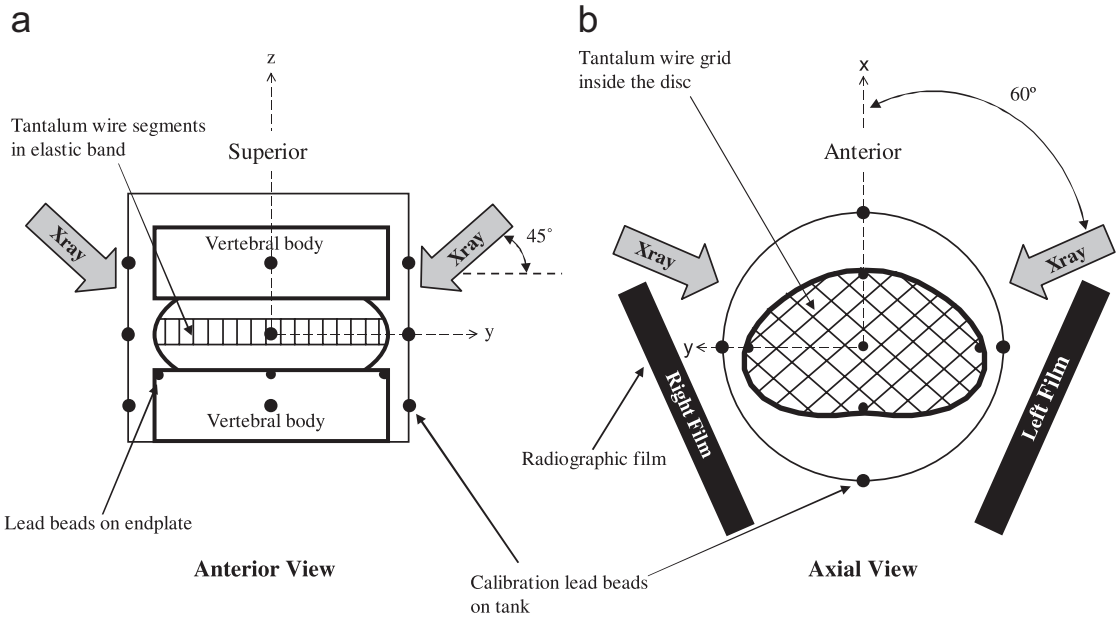

Fig. 1. Schematic of the 3-D stereo-radiography displacement measurement set up. Anterior (a) and axial views (b) show the grid of tantalum wires in the disc, endplate and calibration lead beads, and tantalum wire segments in the elastic band stretched around the periphery of the disc. Stereo-radiographs were taken before and after imposition of displacements/rotations in each of the three principal translations and rotation directions. Specimen fixation cups are not shown and diagrams are not to scale.

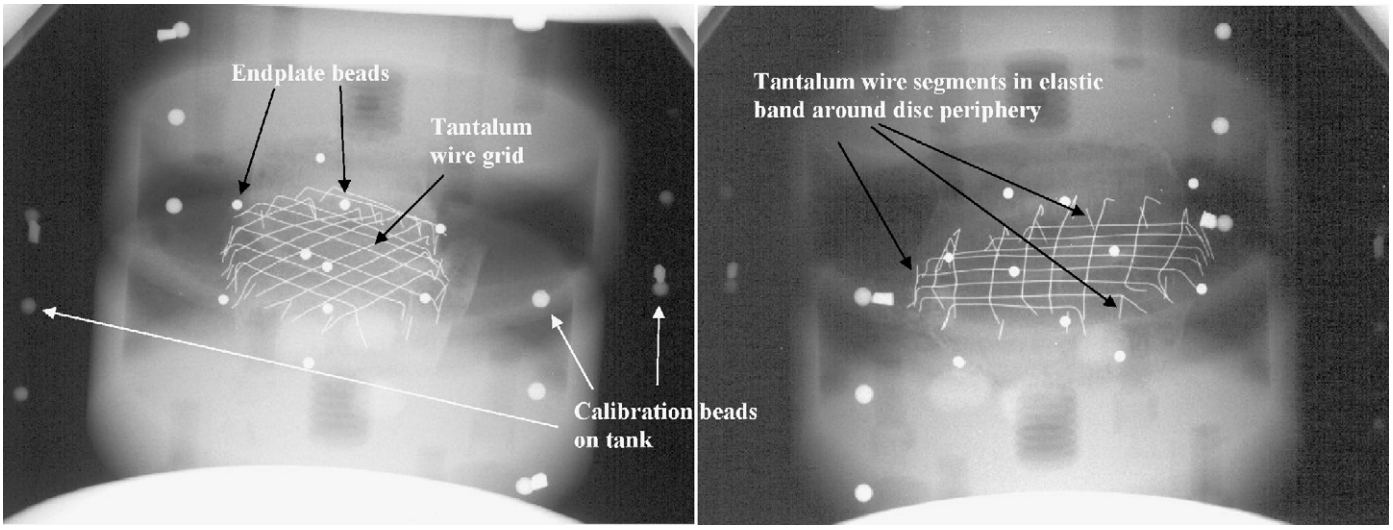

Fig. 2. Left/right stereo-radiograph pair showing the grid of wires in the disc, endplate and calibration beads, and peripheral disc wire segments. *Note*: A total of 10 endplate beads are visible, however, five upper endplate beads were inserted but not used for calculations in this study. Reference in the text is only made to the five lower endplate beads.

z-direction was calculated as $\Delta Z/Z_0$ where ΔZ was the displaced to undisplaced change in the z-distance of each grid node, and Z_0 was the undisplaced (datum position) distance from the node to the inferior endplate plane. The coordinates of the four outer inferior endplate beads were used to define the inferior endplate plane using singular value decomposition. Shear strains in the xz and yz directions were then calculated as the loaded to unloaded Δx and Δy, respectively, of each grid node, divided by Z_0. The three principal strains ($P1$, $P2$, $P3$ where $P1>P2>P3$) and resulting maximum shear strain (MSS) at each grid node were calculated from the 3-D strain tensor (Olsen, 1974), and expressed as %/mm for translation tests and %/° for rotation tests. The digitizing error mentioned previously resulted in a mean (95% CI) precision RMS error for MSS of 0.13% (0.009%).

Mean regional MSS values at each of nine anatomical regions were defined by partitioning the grid. These regions were: anterior (10 nodes), left/right anterolateral (8 nodes each), left/right lateral (6 nodes each), nucleus (15 nodes), left/right posterolateral (8 nodes each), and posterior (8 nodes) (Fig. 3). Regional differences in MSS within each displacement or rotation were identified by a one-way ANOVA and Bonferroni-adjusted post-hoc comparisons. Statistical analyses were performed to evaluate regional differences having the largest MSS only, since shear is considered a likely tissue failure criterion and is derived from principal strains by the formula $(P1-P3)/2$. For each input displacement, the regions with the largest MSS were identified, and the largest regional MSS values were pooled wherever several regions had values that were not significantly different from each other.

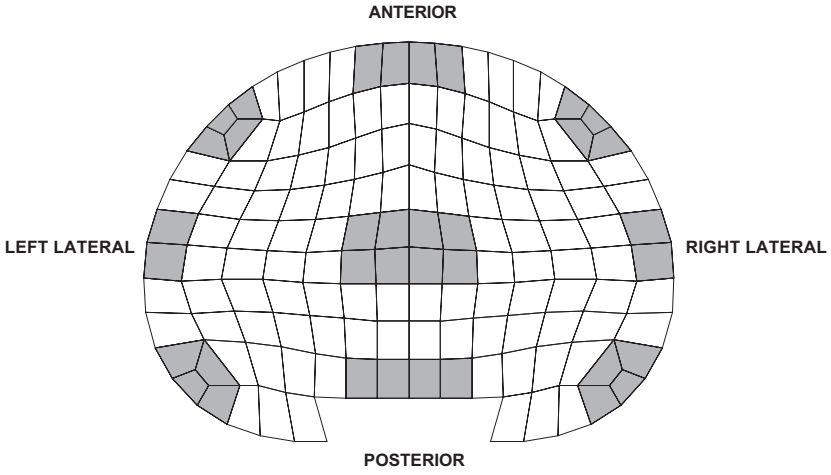

Fig. 3. Axial view of the symmetrical planar intervertebral disc grid used to interpolate displacements and calculate strains. There are 148 four-noded quadrilateral elements. The grid was partitioned into anatomical regions (shaded in gray). Nine regions were defined: anterior, left/right anterolateral, left/right lateral, nucleus, left/right posterolateral and posterior.

To identify the physiological rotations and displacements that may place the disc at greatest risk for large tissue strains and injury, the mean (95% CI) of the pooled regional MSS were multiplied by the maximum reported physiological lumbar segmental motion for each DOF. Use of the largest intersegmental motion (rather than values specific to each anatomical level) represented the 'worst-case' intra-discal strains. The resulting percent MSS for each DOF were then statistically compared. The MSS at the extremes of physiological motion are referred to as physiological MSS.

3. Results

Some individual specimen tests were excluded because of various technical and radiographic problems. The final numbers of specimens for each test were therefore as follows: $N=9$ for right axial rotation and extension, $N=8$ for all shear tests and left lateral bending, $N=7$ for flexion, left axial rotation and right lateral bending, and $N=5$ for compression. The normalized internal disc average displacement vectors in each of the three principal displacement and rotation directions (Fig. 4) serve to confirm the validity of the wire grid technique and form the basis from which MSS were subsequently calculated.

In axial compression, the largest MSS occurred in the lateral, posterior and posterolateral regions of the disc, and was approximately 13%/mm (Fig. 5). In anterior shear, the largest MSS was found in the right anterolateral side and on the right side of the disc (10%/mm). Conversely, in posterior shear, the lateral and posterolateral regions had largest MSS of approximately 11%/mm (Fig. 5). During lateral shear, the largest MSS (12%/mm) was present on the side opposite to the direction of shear (Fig. 5).

The largest MSS (3.5%/°) were similar in flexion and extension. The anterior region had the highest MSS for flexion, and both anterior and posterolateral regions had the highest MSS in extension (Fig. 6). During axial rotation, the largest MSS occurred in the posterolateral side in the direction of rotation (3.5%/°) (Fig. 6). In lateral bending, the posterolateral region, opposite to the side of bending produced the largest MSS (8%/°).

Significant regional variation in MSS was found for all translation and rotation tests ($P<0.001$) (Figs. 7 and 8). The regions of largest regional MSS for each displacement and rotation, are shown in Table 1. In general, the largest regional MSS were found in the posterior, posterolateral and lateral regions of the disc. For the translation motions, lateral shear and compression produced the largest regional MSS per mm of displacement. Lateral shear was significantly larger than anterior and posterior shear ($P<0.015$ for both comparisons), and compression was significantly larger than posterior shear ($P<0.001$). No significant differences existed between compression, lateral shear and anterior shear ($P>0.24$ for all comparisons). For the rotation motions, lateral bending had significantly larger regional MSS per degree of rotation than all other tests ($P<0.001$ for all comparisons), with no significant differences between the remaining rotation motions ($P=1$ for all comparisons).

The physiological MSS produced at the maximum reported lumbar segmental range of motion for each DOF (Table 1) was greatest for lateral bending, which produced physiological MSS that was significantly larger than all other motions, having a mean (95% CI) of 57.8 (16.2)% ($P<0.001$ for all comparisons). In addition, physiological MSS for flexion was also significantly larger than for all remaining motions (38.3 (3.3)%, $P<0.001$ for all comparisons). No significant differences were present between the remaining motions ($P>0.25$ for all comparisons).

4. Discussion

This study provided a comprehensive regional analysis of 3-D intra-discal MSS under three principal displacements

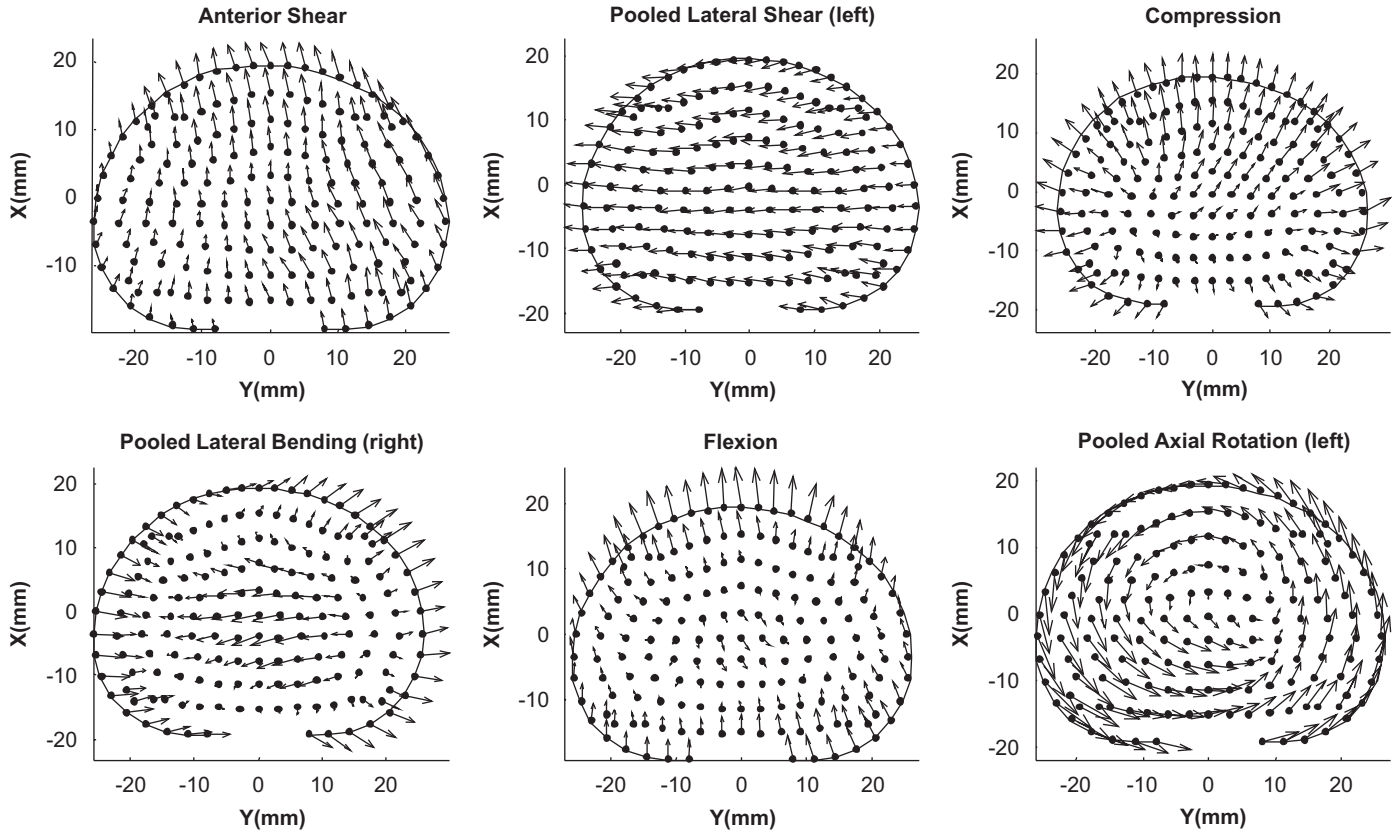

Fig. 4. Normalized internal disc average displacement vectors for anterior shear (Tx), left lateral shear (Ty), compression (Tz), right lateral bending (Rx), flexion (Ry) and left axial rotation (Rz). *Note*: Displacements from symmetrically opposite motions for lateral shear, lateral bending and axial rotation values were pooled, based on presumed sagittal plane symmetry. Translation displacements are magnified 6 ×, and rotation displacements are magnified 30 × for clarity.

and three principal rotations. MSS was chosen as a measure of material strain based on evidence that interlamellar shear strain may play an important role in the creation and propagation of circumferential disc tears (Goel et al., 1995), and that interlamellar shear stresses were found to be relatively large compared to longitudinal and perpendicular fiber stresses, and may therefore contribute to annulus fiber failure (Iatridis and ap Gwynn, 2004; Iatridis et al., 2005).

This study found that lateral shear and compression produced the largest MSS per mm of displacement, with the largest values typically found in the lateral and posterolateral regions of the disc. For the rotation tests, lateral bending produced the largest MSS and these were found in the posterolateral region opposite to the side of bending (the 'tension' side). After calculating the physiological MSS, it was found that lateral bending and flexion were the motions that may place the disc at greatest risk for injury. These findings have been supported by laboratory and epidemiological studies (referenced in the Introduction), but clinically the causes of injury are only speculation. Adding lateral bending to flexion produces the asymmetrical bending that is common in manual handling. This asymmetrical bending may also involve some coupled axial rotation, but axial rotation is not a primary movement of the lumbar spine (Table 1).

The physiological MSS calculated for compression (11.9–13.3%, Table 1) was based on the average displacement reported at endplate failure (Brinckmann et al., 1983), and therefore gives an indication of the level of strain the disc can safely withstand without tissue failure. After taking this 'threshold' level of MSS into account, all motions apart from lateral bending and flexion generate MSS values that lie within this threshold. Lateral bending and flexion generated physiological MSS that were approximately three to four times the threshold during reported physiological motion, although the largest MSS may occur for combined motions. The strains occurring in combined motions may be estimated by employing the principle of superimposition. While the load–displacement behavior of the lumbar spine is non-linear, we performed displacement/rotation controlled tests, where we assumed that for small strains, the displacement–strain behavior was linear and therefore the principal of superposition is valid in this context. Therefore, the combination of a lateral bending and flexion motion may have the highest risk of disc injury. Surprisingly, the MSS and physiological MSS for axial rotations were relatively small.

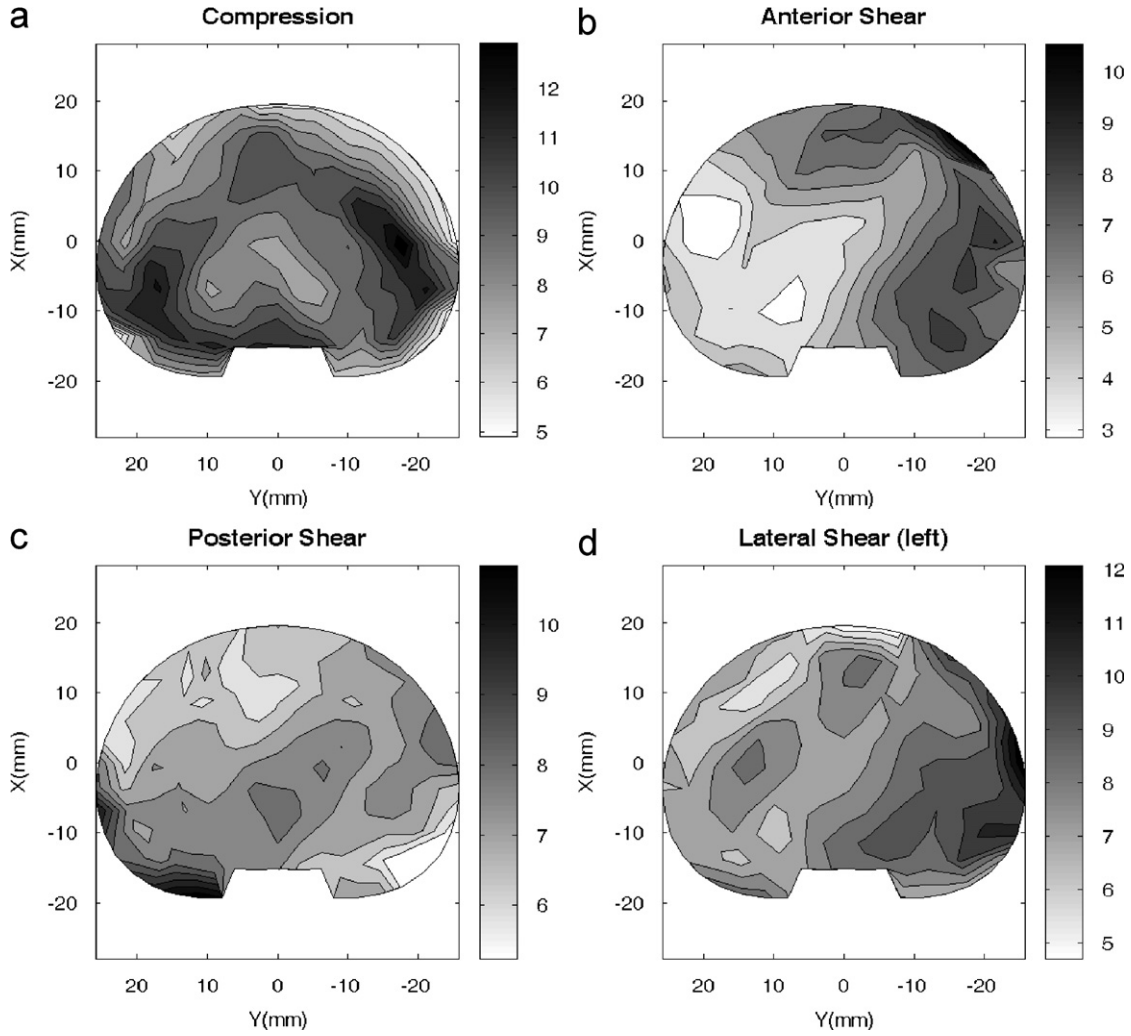

Fig. 5. Contour plots showing the normalized maximum shear strain (%/mm) for translation tests: (a) compression, (b) anterior shear, (c) posterior shear and (d) lateral shear. *Note*: Lateral shear values include pooled values for left and right shear, all presented as if for left shear, based on presumed symmetry.

There were a number of limitations of the methodology employed here. It was difficult to ensure that the specimen was potted perfectly parallel to the disc mid-plane, so some coupling of forces and moments was observed. Also, it was not technically possible to place the grid of wires exactly in the true mid-plane of the disc, which would produce errors in strain measurement. We expected symmetry of strains in axial rotation, lateral bending and lateral shear, based on the expectation that discs have the same geometrical and material properties about the mid-sagittal plane. Individual disc specimens gave strain values that were not exactly symmetrical. These differences were attributed to small misalignment of the specimens in potting the specimens, and/or intra-discal wires not exactly in the mid-plane of the disc. Therefore, we consider the pooled data as a more accurate representation since they would average out the differences due to misaligment. Strains in the z-direction were assumed to be uniform from the central plane of the disc (as marked by wires) to the inferior endplate, which may not apply especially for the relatively large disc deformations occurring in compression and bending.

The use of beads to measure tissue deformation has been previously employed in 2-D radiography studies of internal disc motion (Krag et al., 1987; Seroussi et al., 1989). These methodologies assume that the metallic markers track tissue strain. The individual intra-discal wires may 'slide' relative to the tissue, but the closest approaches 'intersections' between wires are assumed to remain stationary relative to adjacent tissue. The method of using a wire grid in the disc has been extensively validated by Tsantrizos et al. (2005).

The discs used in this study were all grade 1 or 2 by the Thompson subjective grading method. Therefore, the effects of disc degeneration or injury could not be investigated. The invasive method used here could not be employed in vivo or clinically. It is possible that magnetic resonance methods that can 'tag' features of the tissue

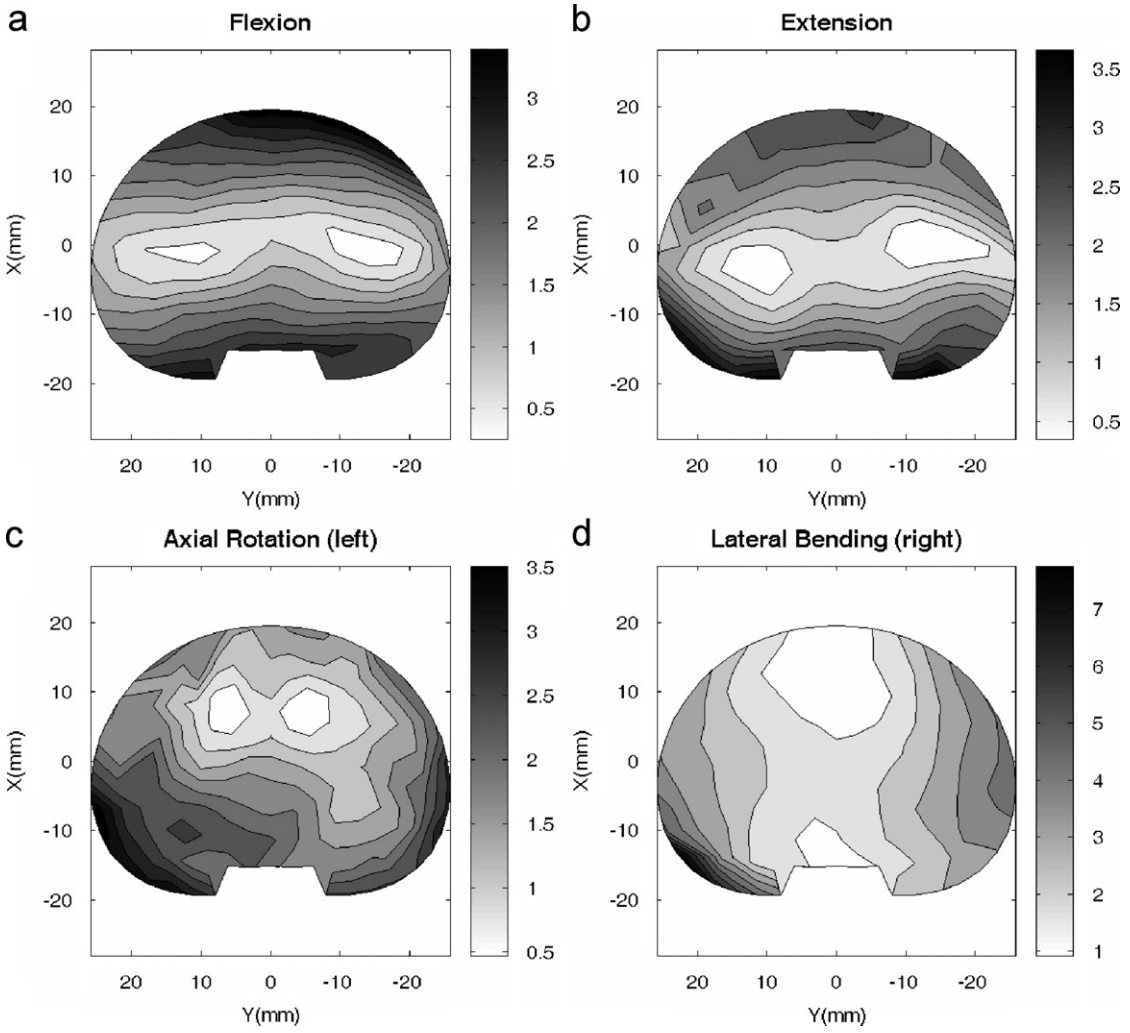

Fig. 6. Contour plots showing the normalized maximum shear strain (%/°) for rotation tests: (a) flexion, (b) extension, (c) axial rotation and (d) lateral bending. *Note*: Values for axial rotation and lateral bending include pooled values for both complementary rotation tests, all presented as if for left axial rotation and right lateral bending respectively, based on presumed symmetry.

might be employed to provide internal displacement data that could be analyzed by similar techniques to measure tissue strain.

Discs were tested after removal of the posterior elements and under displacement control. Physiological strains were inferred by multiplying the normalized strains by reported in vivo ranges of motion between vertebrae. This displacement control approach had the advantages that the results were independent of variations in the tested motion segment flexibility, were not confounded by presence of posterior elements, and did not rely on any estimates of in vivo loading of the spine.

The failure strain of disc annulus fibrosus tested in tension in the circumferential direction has been reported as being between approximately 20% (Acaroglu et al., 1995) and somewhat lower in the fiber direction (Skaggs et al., 1994). Although the method we used to measure intra-discal strain in this study did not directly measure annulus fiber strain, it is of interest to note that the intra-discal strains reported in this study for flexion and lateral bending at the extremes of physiological motion were larger than the failure strain reported for isolated annulus tissue. These differences may suggest that failure of isolated annulus tissue may occur at lower values than for disc annulus in situ.

This study has identified the lumbar segmental motions that produce physiological MSS comparable with the known failure strain of disc tissue and that may place the disc at greatest risk of injury. Lateral bending and flexion place the disc at greatest risk. The exact failure criterion for the intervertebral disc tissues is not known, and MSS was used because it has been shown that disc tears may be initiated by large interlamellar shear strains that dominate over radial and circumferential annular fiber strains. These results provide improved understanding of disc behaviors under loading and may also be of value validating finite element models.

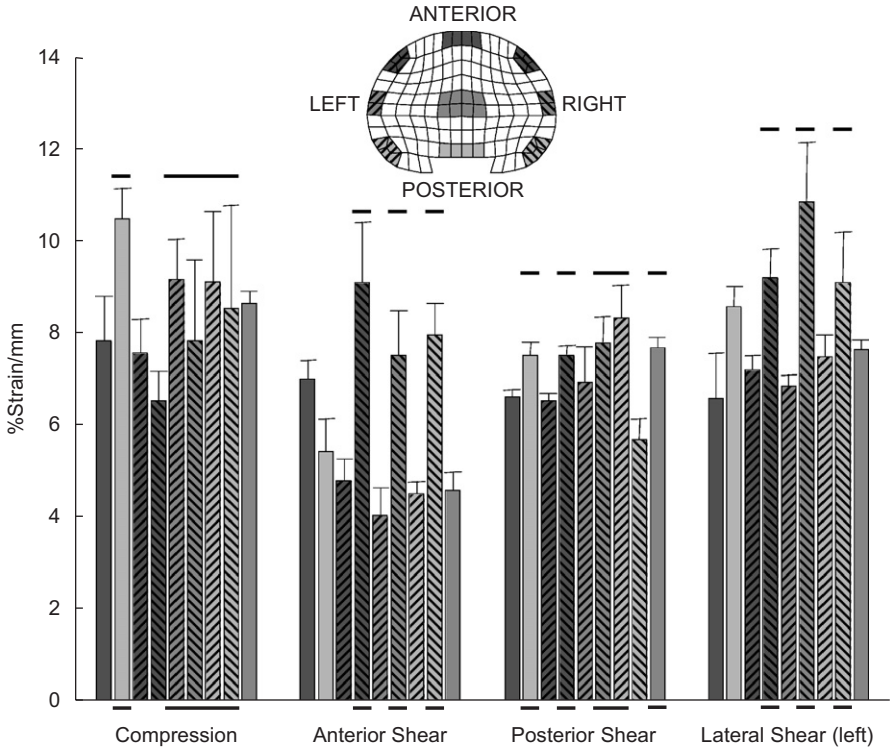

Fig. 7. Mean (95% confidence interval) regional normalized maximum shear strain values for translation tests: axial compression, anterior/posterior shear and lateral shear. *Note*: Lateral shear values include pooled values for left and right shear, all presented as if for left shear, based on presumed symmetry. Bars indicate regions with the largest regional maximum shear strain that are not significantly different.

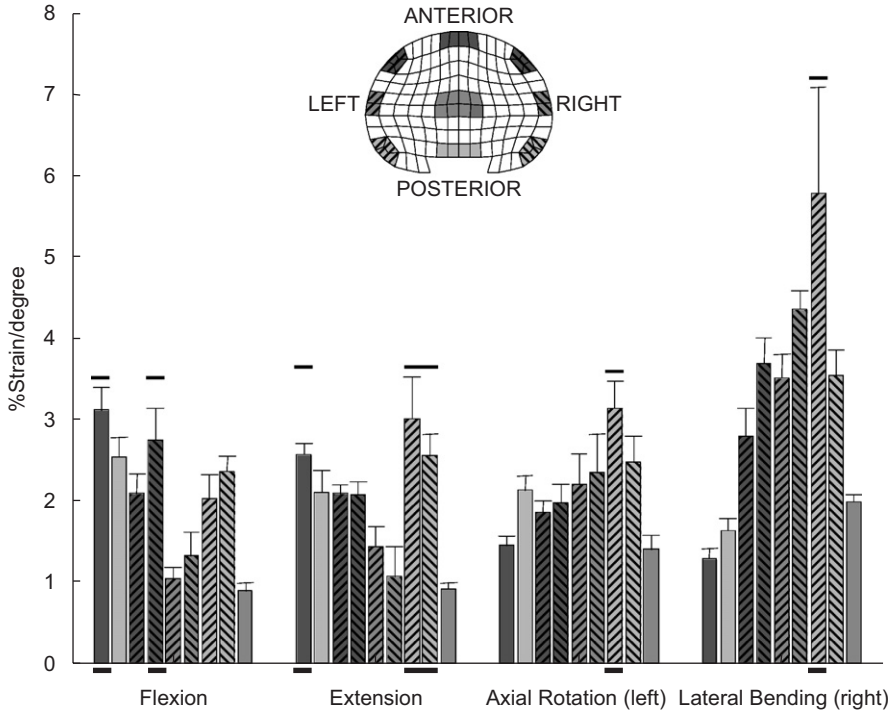

Fig. 8. Mean (95% confidence interval) regional normalized maximum shear strain values for rotation tests: flexion, extension, axial rotation and lateral bending. *Note*: Values for axial rotation and lateral bending include pooled values for both complementary rotation tests, all presented as if for left axial rotation and right lateral bending, respectively, based on presumed symmetry. Bars indicate regions with the largest regional maximum shear strain that are not significantly different.

Table 1
Largest regional maximum shear strains (MSS) and physiological MSS

Input motion	Regions of largest MSS[a]	Largest regional MSS		Maximum reported ROM[b]	Physiological MSS (% strain)	
		Mean	95% confidence interval		Mean	95% confidence interval
Compression	LLat, RLat, LPostLat, RPostLat, Post	9.0%/mm	8.5–9.5%/mm	1.4 mm	12.6	11.9–13.3
Anterior shear	RAntLat, RLat, RPostLat	8.2%/mm	7.6–8.9%/mm	1.4 mm	11.5	10.6–12.5
Posterior shear	RAntLat, RLat, LPostLat, Nucleus, Post	7.7%/mm	7.5–7.9%/mm	1.5 mm	11.6	11.3–11.9
Lateral shear	RAntLat, RLat, RPostLat	9.6%/mm	8.9–10.3%/mm	1.5 mm	14.4	13.4–15.5
Flexion	Ant, RAntLat	2.9%/°	2.7–3.2%/°	13°	38.3	35.1–41.6
Extension	Ant, LPostLat, RPostLat	2.7%/°	2.5–2.9%/°	5°	13.5	12.5–14.5
Axial rotation	LPostLat	3.1%/°	2.7–3.5%/°	3°	9.4	8.1–10.5
Lateral bending	LPostLat	5.8%/°	4.2–7.4%/°	10°	57.8	42.0–74.0

Several regions are listed wherever there were no significant differences between the largest MSS in those regions. Physiological MSS is the largest Regional MSS multiplied by the maximum reported range of motion (ROM).

[a]Regions are denoted as follows: RAntLat: right anterolateral, LLat: left lateral, RLat: right lateral, LPostLat: left posterolateral, RPostLat: right posterolateral, Post: posterior.

[b]Source of maximum ROMs: compression—displacement at endplate failure (Brinckmann et al., 1983), anterior/posterior shear—(Lu et al., 2005), lateral shear—no data found, estimated to be 1.5 mm. Flexion—(Pearcy et al., 1984; Stokes and Frymoyer, 1987), extension—(Pearcy et al., 1984), axial rotation to one side—(Pearcy and Tibrewal, 1984; White and Panjabi, 1990), lateral bending to one side—(Pearcy and Tibrewal, 1984; White and Panjabi, 1990).

Acknowledgments

Dr. Anthony Tsantrizos and Dr. Thomas Steffen (McGill University, Montreal, Canada) developed the concept of using wires in the discs to calculate internal displacements, and loaned the device for wire insertion. Mr. Jake Lubinski (University of Vermont) scanned and digitized the radiographs. Dr. Niclas Börlin (RSA Sweden) kindly made available his Matlab code (functions hungarian.m and condass.m) for determining the best matching endplate bead image pairs. Dr. Peter Kovesi, School of Computer Science & Software Engineering, The University of Western Australia for the Matlab function for fitting a plane using singular value decomposition (function fitplane.m). Spinal specimens were provided by National Disease Research Interchange (NDRI). This study was supported by NIH R01 AR 49370.

References

Acaroglu, E.R., Iatridis, J.C., Setton, L.A., Foster, R.J., Mow, V.C., Weidenbaum, M., 1995. Degeneration and aging affect the tensile behavior of human lumbar anulus fibrosus. Spine 20 (24), 2690–2701.

Adams, M.A., Hutton, W.C., 1982. Prolapsed intervertebral disc. A hyperflexion injury 1981 Volvo Award in Basic Science. Spine 7 (3), 184–191.

Adams, M.A., Hutton, W.C., 1983. The effect of fatigue on the lumbar intervertebral disc. Journal of Bone and Joint Surgery [Br.] 65 (2), 199–203.

Adams, M.A., Hutton, W.C., 1985. Gradual disc prolapse. Spine 10 (6), 524–531.

Adams, M.A., Green, T.P., Dolan, P., 1994. The strength in anterior bending of lumbar intervertebral discs. Spine 19 (19), 2197–2203.

Adams, M.A., Freeman, B.J., Morrison, H.P., Nelson, I.W., Dolan, P., 2000. Mechanical initiation of intervertebral disc degeneration. Spine 25 (13), 1625–1636.

Brinckmann, P., Frobin, W., Hierholzer, E., Horst, M., 1983. Deformation of the vertebral end-plate under axial loading of the spine. Spine 8 (8), 851–856.

Callaghan, J.P., Mcgill, S.M., 2001. Intervertebral disc herniation: studies on a porcine model exposed to highly repetitive flexion/extension motion with compressive force. Clinical Biomechanics (Bristol., Avon.) 16 (1), 28–37.

Dansereau, J., Stokes, I.A., 1988. Measurements of the three-dimensional shape of the rib cage. Journal of Biomechanics 21 (11), 893–901.

Goel, V.K., Monroe, B.T., Gilbertson, L.G., Brinckmann, P., 1995. Interlaminar shear stresses and laminae separation in a disc. Finite element analysis of the L3-L4 motion segment subjected to axial compressive loads. Spine 20 (6), 689–698.

Gordon, S.J., Yang, K.H., Mayer, P.J., Mace Jr., A.H., Kish, V.L., Radin, E.L., 1991. Mechanism of disc rupture. A preliminary report. Spine 16 (4), 450–456.

Iatridis, J.C., ap Gwynn, I., 2004. Mechanisms for mechanical damage in the intervertebral disc annulus fibrosus. Journal of Biomechanics 37 (8), 1165–1175.

Iatridis, J.C., Maclean, J.J., Ryan, D.A., 2005. Mechanical damage to the intervertebral disc annulus fibrosus subjected to tensile loading. Journal of Biomechanics 38 (3), 557–565.

Kelsey, J.L., Githens, P.B., White III, A.A., Holford, T.R., Walter, S.D., O'connor, T., Ostfeld, A.M., Weil, U., Southwick, W.O., Calogero, J.A., 1984. An epidemiologic study of lifting and twisting on the job and risk for acute prolapsed lumbar intervertebral disc. Journal of Orthopaedic Research 2 (1), 61–66.

Krag, M.H., Seroussi, R.E., Wilder, D.G., Pope, M.H., 1987. Internal displacement distribution from in vitro loading of human thoracic and lumbar spinal motion segments: experimental results and theoretical predictions. Spine 12 (10), 1001–1007.

Lu, W.W., Luk, K.D., Holmes, A.D., Cheung, K.M., Leong, J.C., 2005. Pure shear properties of lumbar spinal joints and the effect of tissue sectioning on load sharing. Spine 30 (8), E204–E209.

Marras, W.S., Lavender, S.A., Leurgans, S.E., Rajulu, S.L., Allread, W.G., Fathallah, F.A., Ferguson, S.A., 1993. The role of dynamic three-dimensional trunk motion in occupationally-related low back disorders. The effects of workplace factors, trunk position, and trunk motion characteristics on risk of injury. Spine 18 (5), 617–628.

Marras, W.S., Davis, K.G., Ferguson, S.A., Lucas, B.R., Gupta, P., 2001. Spine loading characteristics of patients with low back pain compared with asymptomatic individuals. Spine 26 (23), 2566–2574.

Mcgill, S.M., Hughson, R.L., Parks, K., 2000. Changes in lumbar lordosis modify the role of the extensor muscles. Clinical Biomechanics (Bristol., Avon.) 15 (10), 777–780.

Miller, J.A., Schultz, A.B., Warwick, D.N., Spencer, D.L., 1986. Mechanical properties of lumbar spine motion segments under large loads. Journal of Biomechanics 19 (1), 79–84.

Norman, R., Wells, R., Neumann, P., Frank, J., Shannon, H., Kerr, M., 1998. A comparison of peak vs cumulative physical work exposure risk factors for the reporting of low back pain in the automotive industry. Clinical Biomechanics (Bristol., Avon.) 13 (8), 561–573.

Olsen, G.A., 1974. Elements of mechanics of materials. 3rd ed. Englewood Cliffs, NJ, Prentice-Hall, pp. 485–500.

Pearcy, M., Portek, I., Shepherd, J., 1984. Three-dimensional x-ray analysis of normal movement in the lumbar spine. Spine 9 (3), 294–297.

Pearcy, M.J., Tibrewal, S.B., 1984. Axial rotation and lateral bending in the normal lumbar spine measured by three-dimensional radiography. Spine 9 (6), 582–587.

Reinschmidt, C., van den Bogert, T., 1997. KineMat. A MATLAB Toolbox for Three-Dimensional Kinematic Analyses. Human Performance Laboratory, The University of Calgary 〈http://isbweb.org/software/movanal/kinemat/index.html〉. Last accessed: 31st May 2006.

Seroussi, R.E., Krag, M.H., Muller, D.L., Pope, M.H., 1989. Internal deformations of intact and denucleated human lumbar discs subjected to compression, flexion, and extension loads. Journal of Orthopaedic Research 7 (1), 122–131.

Shirazi-Adl, A., 1989. Strain in fibers of a lumbar disc. Analysis of the role of lifting in producing disc prolapse. Spine 14 (1), 96–103.

Skaggs, D.L., Weidenbaum, M., Iatridis, J.C., Ratcliffe, A., Mow, V.C., 1994. Regional variation in tensile properties and biochemical composition of the human lumbar anulus fibrosus. Spine 19 (12), 1310–1319.

Steffen, H.G., Baramki, H.G., Rubin, R., Antoniou, M., Aebe, M., 1998. Lumbar intradiscal pressure measured in the anterior and posterolateral annular regions during asymmetrical loading. Clinical Biomechanics 13 (7), 495–505.

Stokes, I.A., Frymoyer, J.W., 1987. Segmental motion and instability. Spine 12 (7), 688–691.

Stokes, I.A., Gardner-Morse, M., Churchill, D., Laible, J.P., 2002. Measurement of a spinal motion segment stiffness matrix. Journal of Biomechanics 35 (4), 517–521.

Thompson, J.P., Pearce, R.H., Schechter, M.T., Adams, M.E., Tsang, I.K., Bishop, P.B., 1990. Preliminary evaluation of a scheme for grading the gross morphology of the human intervertebral disc. Spine 15 (5), 411–415.

Tsantrizos, A., Ito, K., Aebi, M., Steffen, T., 2005. Internal strains in healthy and degenerated lumbar intervertebral discs. Spine 30 (19), 2129–2137.

Vernon-Roberts, B., Pirie, C.J., 1977. Degenerative changes in the intervertebral discs of the lumbar spine and their sequelae. Rheumatology and Rehabilitation 16 (1), 13–21.

Vernon-Roberts, B., Fazzalari, N.L., Manthey, B.A., 1997. Pathogenesis of tears of the anulus investigated by multiple-level transaxial analysis of the T12-L1 disc. Spine 22 (22), 2641–2646.

White 3rd, A.A., Panjabi, M.M., 1990. Clinical Biomechanics of the Spine: J.B. Lippincott Company.